A control-theoretic outlook at the no-go zone in sailing vessels

Article · January 2011

3 authors, including:

Jerome Jouffroy
University of Southern Denmark
62 PUBLICATIONS **574** CITATIONS

A control-theoretic outlook at the no-go zone in sailing vessels

Bin Yang†, Lin Xiao‡, and Jerome Jouffroy‡
Mads Clausen Institute
University of Southern Denmark (SDU)
Alsion 2, DK-6400, Sønderborg, Denmark
Email: † biyan09@student.sdu.dk; ‡ {xiao, jerome}@mci.sdu.dk

***Abstract*—Sailing vessels, due to their particular propulsive mechanism, gradually lose power as they face the wind, i.e. when they are in the so-called "no-go zone". Interestingly, dynamical models of sailing vessels, which are usually quite complex, all have in common this no-go zone effect. Using a control-theoretic concept called backward reachable set, we demonstrate how a much simpler dynamic model that we proposed in an earlier study, has very similar dynamic properties as that of its most complex counterparts. This model comparison is done through theoretical validation and computation of their reachable sets.**

I. Introduction

In our fast developing world, the realization of our limited resources, as well as the need for protection of our environment have been attracting more and more attention. Nowadays, investigations toward renewable energies and low-carbon applications are become more popular. Sailing vessels, which are driven by the wind, have clean technological and energy saving potentials, in contrast to more conventional propulsion means such as propellers and thrusters. Although human beings have over the centuries accumulated a considerable wealth of knowledge on navigation, architecture and many other aspects of sailing vessels, a very limited number of studies were dedicated to automatic control of sailing vessels.

A significant characteristic of sailing is that a vessel will lose the propulsive force from the environment as it enters the so-called "no-go zone", and it will be able to cross this deadzone using only its inertia. When performing a tacking maneuver[1], a vessel might get stuck or be "in irons", if its speed before entering the no-go zone is too slow to cross it entirely. Clearly, such situation should be avoided. In control theoretic terms, the sailing vessel must stay out of a so-called *backward reachable set*, which is a set including all states that lead the vessel to a final state represented by the vehicle with a heading in the no-go zone and a zero velocity. Otherwise, a sailing vessel with a state belonging to the reachable set is guaranteed to eventually be in irons.

Dynamic models of sailing yachts are generally quite complex, including aero- and hydrodynamics of the hull and the different appendages (i.e. sail, keel, rudder), and might not always be suitable for controller design or path planning strategies. For this reason, a simpler phenomenon-based model, which we refer to here as "deadzone" model, was introduced in [1] to represent the dynamics of many sailing vessels, in which the key element is an idealized form of a polar performance diagram. As general and simple as it is, the deadzone model was used in studies on motion planning for maneuvers such as tacking [1] or wearing [2].

In the proposed paper, we test the validity of the deadzone model by comparing its backward reachable set corresponding to the no-go zone against that of another relatively simple model of a sailing vehicle, the latter being based on a more conventional lift/drag description for the sail. For each model, the reachable set is numerically computed by solving a particular Hamilton-Jacobi (HJ) Partial Differential Equation, similarly to [3]. The two sets being very similar is an indication that the simple deadzone model represents sailing vehicles well enough around the no-go zone, which in our view is the essence of maneuvers in sailing.

After this introduction, section 2 will be dedicated to the presentation of the deadzone model and the lift/drag model, both of which consisting of a basic kinematic structure and dynamics induced by combining the inertia of the vehicle with a propulsive component. After recalling the concepts of reachable and target set in section 3, we will make a reachable set analysis of the two models by using the HJ PDE method. After showing how the sets are derived and computed, they are then compared to one another. Finally, concluding remarks end this paper.

II. Simple models of surface sailing vessels

Instead of deriving a full model of a particular sailing vessel based on first principles (see for example in [4] for conventional ships), we would like to have at our disposal a model that would be as simple as possible to gain insights of the problem at hand. To this end, we consider that a sailing vessel may be modelled by a simple kinematic vehicle, with sail/wing as the part responsible for propulsion. Following our previous work (see [1][2]), we hence use the following set of differential equations

$$\dot{x}(t) = v_u(t)\cos\theta(t) \tag{1}$$

$$\dot{y}(t) = v_u(t)\sin\theta(t) \tag{2}$$

$$\dot{\theta}(t) = \frac{v_u(t)}{L}\tan\delta_r(t), \tag{3}$$

[1]which is done when going upwind by zigzagging and during which the sailing vessels have to go across the no-go zone.

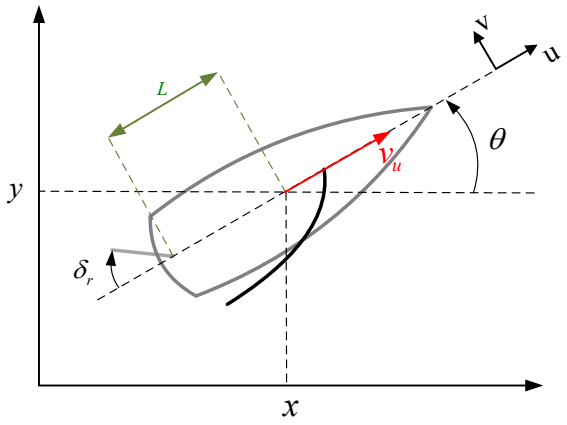

Fig. 1. The model for the sailing vessel

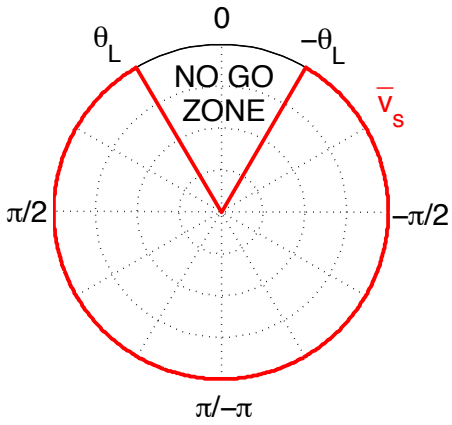

Fig. 2. Polar curve of the propulsive system

where (x, y) is the position of the vessel in the earth-fixed frame, θ is the heading angle, v_u represents the longitudinal velocity or surge velocity. Angle δ_r denotes the input corresponding to the rudder angle, which is assumed to lie within the interval $[-\bar{\delta}_r, \bar{\delta}_r]$, with $0 < \bar{\delta}_r < \pi/2$. Constant L is a length parameter related to the maximum curvature of the path taken by the vessel.

A. Deadzone Model

The deadzone model simply consists in combining dynamics (1)-(3) with dynamics in v_u that captures the essence of the dynamic behavior of sailing vessels. The dynamics in v_u can be simply described by the following expression

$$m\dot{v}_u(t) + dv_u(t) = d\rho(\theta(t), v_s(t)), \tag{4}$$

where m is the mass of the vessel and d is a linear damping term in surge. Function $\rho(\theta(t), v_s(t))$ plays the role of a performance polar diagram, well-known in the sailing world, which gives the maximum feasible velocity of the vessel depending both on its orientation $\theta(t)$ and on the way the sail is trimmed, represented by control input $v_s(t)$. Although $\rho(\theta(t), v_s(t))$ can take many different and complex shapes (see for example in [5], [6]), we assume that

$$\rho(\theta(t), v_s(t)) = \begin{cases} 0 & \text{if } |\theta(t)| \leq \theta_L \\ sat_{\bar{v}_s}(v_s(t)) & \text{otherwise} \end{cases} \tag{5}$$

where $\bar{v}_s$ is the maximum velocity the vessel can reach and is dependent on the wind velocity. Fig. 2 represents function (5).

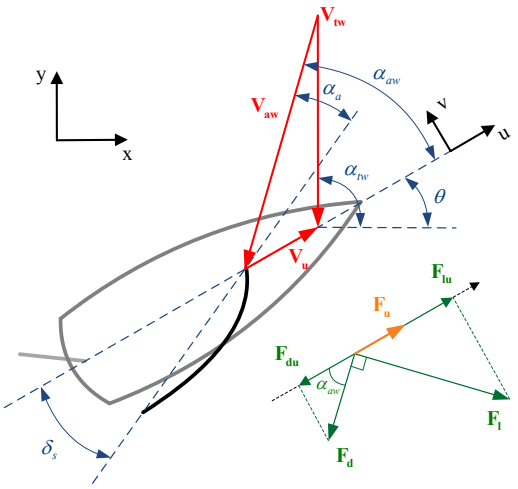

Fig. 3. Wind velocity triangle and aerodynamic forces

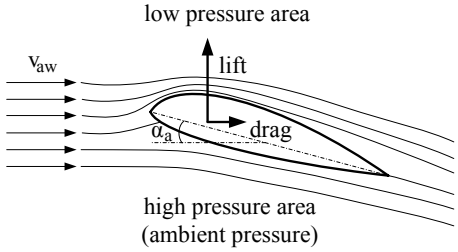

Fig. 4. Lift and drag forces generated on an airfoil under a certain angle of attack α_a.

B. Lift/Drag Model

A more conventional way of modeling the propulsive part of sailing vehicles is to model the sail as a wing, and to take, as the driving force, a projection of the lift and drag forces (see Fig. 3). Thus, we propose the following equation to model the velocity dynamics:

$$m\dot{v}_u(t) + dv_u(t) = F_u(\theta(t), v_u(t), \bar{\delta}_s(t)), \tag{6}$$

where $\bar{\delta}_s$ is a parameter representing the trimming of the sail. The quantity F_u denotes the longitudinal aerodynamic force propelling the vessel, which is generated from the interaction between the wind and the sail.

In the following, we consider that a sail can be seen as an airfoil [5] with similar aerodynamics as the wing of a plane. The lift and drag forces result from the motion between the foil and the fluid, both of which are acting on the foil (see Fig. 4) and vary according to the angle of attack α_a.

The wind velocity and aerodynamic forces are represented in Fig. 3, assuming that the lift and drag forces act directly on the vessel's reference point (x, y). The true wind coming from the north is indicated by the velocity vector $\mathbf{V_{tw}}$, which, in the present paper, is fixed and defined in the earth-fixed frame. The apparent wind velocity $\mathbf{V_{aw}}$ is a vector sum of the true wind velocity $\mathbf{V_{tw}}$ and the longitudinal velocity of the vessel $\mathbf{V_u}$. Hence

$$\mathbf{V_{aw}} = \mathbf{V_{tw}} - \mathbf{V_u}, \tag{7}$$

where the angle between the horizontal x-axis and the true wind is the true wind angle α_{tw}, while the angle between the longitudinal u-axis and the apparent wind is called apparent wind angle and is denoted as α_{aw}. Transform now $\mathbf{V_{tw}} = [v_{twx}, v_{twy}]^T$ from the earth-fixed frame into $\mathbf{V_{tw}^b} = [v_{twu}, v_{twv}]^T$ in the body-fixed frame via a rotation by $-\theta$, i.e.

$$\mathbf{V_{tw}^b} := \begin{bmatrix} v_{twu} \\ v_{twv} \end{bmatrix} = \mathbf{R}\mathbf{V_{tw}}, \tag{8}$$

where the rotation matrix $R(-\theta)$ is given by

$$\mathbf{R}(-\theta) = \begin{bmatrix} \cos\theta & \sin\theta \\ -\sin\theta & \cos\theta \end{bmatrix}. \tag{9}$$

Hence, the velocity vector $\mathbf{V_{aw}}$ in (7) can be calculated as

$$\mathbf{V_{aw}} = \begin{bmatrix} v_{awu} \\ v_{awv} \end{bmatrix} = \begin{bmatrix} v_{twu} \\ v_{twv} \end{bmatrix} - \begin{bmatrix} v_u \\ 0 \end{bmatrix}, \tag{10}$$

from which we get the apparent wind amplitude $v_{aw} = \sqrt{v_{awu}^2 + v_{awv}^2}$ and the apparent wind angle

$$\alpha_{aw} = \arctan 2(-v_{awv}, -v_{awu}), \tag{11}$$

where $\arctan 2$ returns the four-quadrant inverse tangent of vector $[-v_{awu}, -v_{awv}]^T$, which is limited to the interval $(-\pi, \pi]$.

The angle of attack α_a can be related to the apparent wind angle through the following expression (see also Fig. 3)

$$\alpha_a = \alpha_{aw} - \delta_s, \tag{12}$$

where δ_s is the sail angle. Then, the lift and drag forces can be expressed as (see [5])

$$F_l = \frac{1}{2}\rho v_{aw}^2 S C_l(\alpha_a) \tag{13}$$

$$F_d = \frac{1}{2}\rho v_{aw}^2 S C_d(\alpha_a), \tag{14}$$

where S is the sail area, ρ is the density of the fluid, $C_l(\alpha_a)$ and $C_d(\alpha_a)$ are the so-called lift and drag coefficients represented in Fig. 5 (see also [5]). The projection of $\mathbf{F_l}$ and $\mathbf{F_d}$ on the u-axis constitute the propulsive force, which is written as

$$F_u = F_l \sin\alpha_{aw} - F_d \cos\alpha_{aw}. \tag{15}$$

Hence, the longitudinal driving force for the lift/drag model is given by

$$F_u = \frac{1}{2}\rho v_{aw}^2 S\big(C_l(\alpha_a)\sin\alpha_{aw} - C_d(\alpha_a)\cos\alpha_{aw}\big). \tag{16}$$

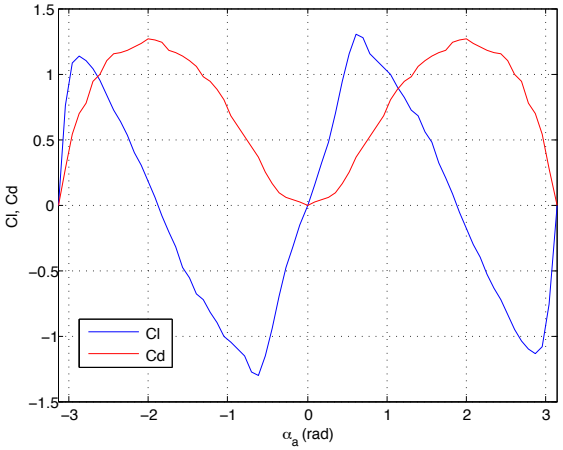

Fig. 5. Lift and drag coefficients

In addition, when in a tacking maneuver, the sail typically loses lift and starts luffing. As a consequence, the tension of the rope connecting the sail (or usually the boom) with the boat also disappears, letting the rope loose. In this situation, the sail becomes aligned with the apparent wind, i.e. the angle of attack $\alpha_a = 0$. It stays like this until the rope is in tension again, i.e. when the apparent wind angle is greater than the maximum allowed sail angle, as set by the rope length. To model this behavior, we then use the following expression

$$\delta_s = \begin{cases} \pm\bar{\delta}_s & \text{if } |\alpha_{aw}| > \bar{\delta}_s \\ \alpha_{aw} & \text{otherwise} \end{cases} \tag{17}$$

where $\bar{\delta}_s$ is the maximum sail angle with $0 < \bar{\delta}_s < \pi/2$.

III. Reachable Set Analysis

A. Reachable set and computation with a PDE

Whether or not a sailing vessel will get stuck in the no-go zone when tacking is important for an autonomous sailing vehicle. In the worst case, once stuck "in irons", a sailboat typically goes backwards, increases backward velocity to gain steerage, before finally getting a heading allowing to re-capture some wind again and sail forward.

Ending up being in irons happens when the velocity before the tack is not sufficient. A simple way to check whether a particular state of the ship (i.e. particular heading and velocity) will eventually lead to the vehicle being in irons is to run a simulation with this particular state as an initial condition to see whether the system eventually stops. However, it only gives us information on one single trajectory. For systems with many possible states and input signals, it is not practical or efficient to check every trajectory.

Alternatively, direct computation of the reachable set which encompasses all trajectories satisfying a certain property is more appropriate. A *backward reachable set* is the set of the states from which the trajectories can reach a *target set* we want to avoid [7]. In our case, the target set is the set of configurations for which the vehicle has zero velocity and

when the wind cannot propel the vehicle forward, i.e. when the heading lies in the no-go zone.

In order to obtain numerically the backward reachable sets corresponding to our models, we used an algorithm proposed by Mitchell and co-authors [3] which, roughly speaking, consists in computing the solution of a specific time-dependent Hamilton-Jacobi partial differential equation, by taking as initial condition of the PDE the target set of the no-go zone.

However, before giving the PDE used to compute the reachable sets, let us first clarify mathematically a few elements. First, note that while the behavior of the vehicle around the no-go zone is determined by the state components θ and v_u, it is in fact independent from the actual position (x, y), as getting stuck in the no-go zone can happen for any position. Hence for our reachability analysis, we only need to consider a reduced set of equations represented as follows:

$$\frac{d\mathbf{x}}{dt} = \dot{\mathbf{x}} = f(\mathbf{x}, \delta_r, u^\star), \tag{18}$$

where $\mathbf{x} = [\theta, v_u]^T$. Variable $\delta_r \in [-\bar{\delta}_r, \bar{\delta}_r]$ is the rudder angle, $u^\star \in [\underline{u}, \bar{u}]$ represents the other control variable, i.e. the velocity $v_s \in [0, \bar{v}_s]$ in the deadzone model or the maximum sail angle $\bar{\delta}_s \in [0, \pi/2]$ in the lift/drag model.

In the following, we assume that the sailing vehicle turns with a fixed rudder angle δ_r and a particular $u^\star$. We write a solution of (18) along time variable r as [8]:

$$\mathbf{x}(r, \mathbf{x}_t, \delta_r, u^\star) : [t, 0] \to \mathbb{R}^2,$$

where $\mathbf{x}(t) = \mathbf{x}_t$ is, in the present case, seen as the initial condition, i.e. trajectory $\mathbf{x}(r, \mathbf{x}_t, \delta_r, u^\star)$ starts at the initial time $t < 0$ and ends at time zero, and r is defined on interval $[t, 0]$. Furthermore, we also assume that the target set $\mathbf{G}_0 \subset \mathbb{R}^2$ in our reachability problem is closed and can be represented as the subzero level set of a bounded and Lipschitz continuous function $g : \mathbb{R}^2 \to \mathbb{R}$ [3]

$$\mathbf{G}_0 = \{\mathbf{x} \in \mathbb{R}^2 \mid g(\mathbf{x}) \leq 0\}. \tag{19}$$

The reachable set should contain all trajectories that pass through the target set at some point in time. Hence, define τ as the length of the interval $[t, 0]$, i.e. $\tau = -t$, and let s denote an instant on interval $[t, 0]$. Then, the backward reachable set for $\tau \in [0, T]$ $(T > 0)$ is defined as

$$\mathbf{G}(\tau) = \{\mathbf{x} \in \mathbb{R}^2 \mid \exists s \in [t, 0], \mathbf{x}(s, \mathbf{x}_t, \delta_r, u^\star) \in \mathbf{G}_0\}. \tag{20}$$

Thus, the backward reachable set $\mathbf{G}(\tau)$ includes all states from which the trajectories lead to the target set within time τ in (20).

After these few preliminaries, we are now ready to compute the reachable set (20) for our problem, by calculating the viscosity solution [9] of a time dependent HJ equation, given in the theorem below.

***Theorem** 1:* Let $\phi : \mathbb{R}^2 \times [-T, 0] \to \mathbb{R}$ be the viscosity solution of the HJ PDE

$$\frac{\partial \phi}{\partial t}(\mathbf{x}, t) = -\min\left(0, H(\mathbf{x}, \frac{\partial \phi}{\partial \mathbf{x}}(\mathbf{x}, t)\right)$$
$$\phi(\mathbf{x}, 0) = g(\mathbf{x}) \tag{21}$$

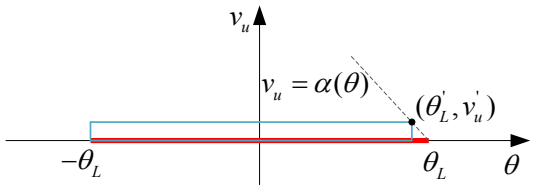

Fig. 6. Target set for the deadzone model

where

$$H(\mathbf{x}, p) = \max_{\delta_r}[p^T f(\mathbf{x}, \delta_r, u^\star)], \; p = \frac{\partial \phi}{\partial \mathbf{x}}(\mathbf{x}, t). \tag{22}$$

Then the subzero level set of ϕ describes $\mathbf{G}(\tau)$, i.e. we have

$$\mathbf{G}(\tau) = \{\mathbf{x} \in \mathbb{R}^2 \mid \phi(\mathbf{x}, t) \leq 0\}. \tag{23}$$

The proof of this theorem is given in [3].

Hence, by computing the solution $\phi(\mathbf{x}, t)$ of PDE (21) initialized with $g(\mathbf{x})$, we get the reachable set for system (18) (through the definition of Hamiltonian (22)). Numerically, a family of algorithms referred to as *level set methods* [10], [11] are used to approximate the viscosity solution of the PDE in (21). The algorithms were implemented using Mitchell's Matlab toolbox for level set methods [12].

B. Deadzone model reachability analysis

For the deadzone model, vector field f in (18) is expressed as

$$\dot{\mathbf{x}} = \frac{d}{dt}\begin{bmatrix} \theta \\ v_u \end{bmatrix} = \begin{bmatrix} \frac{v_u}{L}\tan\delta_r \\ \frac{1}{m}\big(\rho(\theta, v_s) - dv_u\big) \end{bmatrix} = f(\mathbf{x}, \delta_r, v_s), \tag{24}$$

from which we get the Hamiltonian

$$\begin{aligned} H(\mathbf{x}, p) &= \max_{\delta_r}[p^T f(\mathbf{x}, \delta_r, v_s)] = p^T f(\mathbf{x}, \bar{\delta}_r, v_s) \\ &= p_1 \frac{v_u}{L}\tan\bar{\delta}_r + \frac{p_2}{m}\big(\rho(\theta, v_s) - dv_u\big), \end{aligned} \tag{25}$$

where the parameters are $L = 2$, $m = 150$, $d = 10$, $\theta_L = \pi/3$, $v_s = 2$, $\bar{\delta}_r = \pi/4$.

The target set contains the states of longitudinal velocity $v_u = 0$ with heading angle $-\theta_L \leq \theta \leq \theta_L$ (i.e. the no-go zone in Fig. 2), which, in a plane, is represented as the line segment between points $(-\theta_L, 0)$ and $(\theta_L, 0)$, as illustrated in Fig. 6. Mathematically, we have

$$\begin{aligned} \mathbf{G}_0 &= \{\mathbf{x} \in (-\theta_L \leq \theta \leq \theta_L) \times (v_u = 0) \mid g(\mathbf{x}) \leq 0\}, \\ g(\mathbf{x}) &= \max(|v_u|, |\theta| - \theta_L). \end{aligned} \tag{26}$$

In order to use directly Mitchell's Matlab toolbox [12], we replace the line segment with a rectangle target set in the numerical computation, i.e.

$$\begin{aligned} \mathbf{G}_0 = \{\mathbf{x} \in (-\theta_L \leq \theta \leq \theta_L') \times (0 \leq v_u \leq v_u') \mid g(\mathbf{x}) \leq 0\}, \\ g(\mathbf{x}) = \max\left(\left|\theta - \frac{\theta_L' - \theta_L}{2}\right| - \frac{\theta_L' + \theta_L}{2}, \right. \\ \left. \left|v_u - \frac{v_u'}{2}\right| - \frac{v_u'}{2}\right), \end{aligned} \tag{27}$$

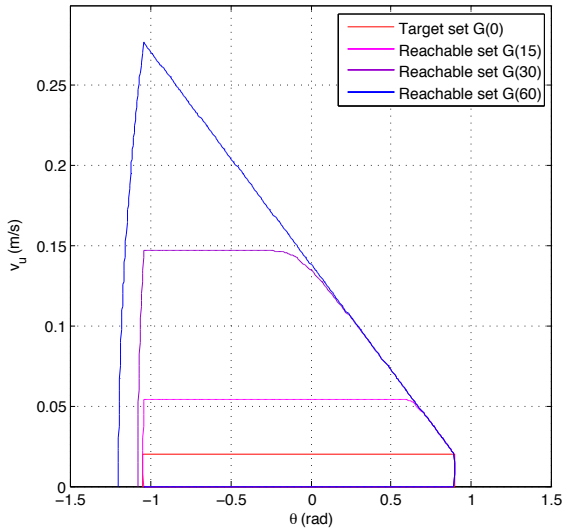

Fig. 7. The reachable set $\mathbf{G}(\tau) = \{\mathbf{x} \in \mathbb{R}^2 \mid \phi \leq 0\}$ for the deadzone model, $\tau = 15, 30, 60s$.

where $v'_u = 0.02$ in our computation (this value should be small enough to ensure a good accuracy). Note that since, for a heading at $\theta = \theta_L$, even a small strictly positive velocity could lead to the vehicle getting out of the no-go zone and re-capture some wind, the rectangular set has to be less large as the line segment, as represented in Fig. 6. As will be demonstrated in the next subsection, this in turn corresponds to a mathematical relation between the limit of the rectangular set θ'_L and v'_u.

As mentioned before, the backward reachable set $\mathbf{G}(\tau)$ contains all states from which the trajectories lead to the target set within time τ. Thus, when τ increases, the reachable set $\mathbf{G}(\tau)$ would enlarge accordingly. The reachable sets for the deadzone model with $\tau = 15, 30, 60s$ are shown in Fig. 7, where we can see them "growing" from the target set.

Obviously, we are interested in determining $\mathbf{G}(\tau)$ for $\tau \to \infty$, noted $\mathbf{G}_\infty$. Numerically, this corresponds to running (21) until $H(\mathbf{x}, \frac{\partial \phi}{\partial \mathbf{x}}(\mathbf{x}, t)) \approx 0$ (with the parameters given above, this occurs around $\tau = 60s$). Then, the final backward reachable set $\mathbf{G}_\infty \approx \mathbf{G}(60)$ associated with the deadzone model is obtained and shown in Fig. 7. As can be seen, the boundary of the reachable set consists of, roughly speaking, a rising curve and a declining curve. The rising curve, on the left side of the no-go zone, represents the minimum velocities needed to cross the no-go zone *before* the vehicle reaches the target set boundary $-\theta_L = -\pi/3$, while the declining curve represents the minimum velocities necessary to cross the no-go zone when the vehicle is *in* it. States *within* the reachable set, which is the area delimited by the curve and the x-axis, will result in the vehicle reaching the target set, i.e. getting stuck in the no-go zone.

C. Theoretical validation

The relatively low complexity of ODE (24) allows us to solve it directly and obtain a trajectory of (θ, v_u) in the state space with initial state (θ_0, v_{u0}), and, as a result, determine accurately the boundary of the reachable set for the deadzone model. Thus, similarly to the work of Mitchell [3], we can check that the PDE reachable set computation method gives accurate results.

Hence, in the following, we give mathematical expressions of the boundaries of the reachable set $\mathbf{G}_\infty$ shown in Fig. 7, where the decreasing right-hand side curve represents a function, $v_u = \alpha(\theta)$, while the increasing curve on the left refers to function $v_u = \beta(\theta)$.

1) Boundary Function $\alpha(\theta)$: When the sailing vessel is already in the no-go zone, i.e. $|\theta| \leq \theta_L$, (24) can be re-written as:

$$\dot{\theta}(t) = \frac{v_u(t)}{L} \tan \delta_r(t) \tag{28}$$

$$\dot{v}_u(t) = -\frac{d}{m} v_u(t). \tag{29}$$

The solution of the first-order ODE (29) with initial condition v_{u0} is obviously

$$v_u(t) = v_{u0} e^{-\frac{d}{m}t}, \tag{30}$$

which gives

$$\dot{\theta} = \frac{v_{u0} \tan \delta_r}{L} e^{-\frac{d}{m}t}. \tag{31}$$

Integrating both sides of (31) and taking into account initial condition θ_0 ($|\theta_0| \leq \theta_L$), we have

$$\begin{aligned} \theta(t) &= \int_0^t \frac{v_{u0} \tan \delta_r}{L} e^{-\frac{d}{m}\tau} d\tau + \theta_0 \\ &= \frac{m v_{u0} \tan \delta_r}{dL} (1 - e^{-\frac{d}{m}t}) + \theta_0. \end{aligned} \tag{32}$$

When $t \to \infty$, (30) and (32) give

$$\lim_{t \to \infty} v_u(t) = 0 \tag{33}$$

and

$$\lim_{t \to \infty} \theta(t) = \frac{m v_{u0} \tan \delta_r}{dL} + \theta_0, \tag{34}$$

respectively. Assume the vessel reaches the end of the no-go zone at infinite time $t \to \infty$, i.e.

$$\lim_{t \to \infty} \theta(t) = \theta_L, \tag{35}$$

then substituting (35) into (34) yields

$$v_{u0} = \frac{dL(\theta_L - \theta_0)}{m \tan \delta_r}. \tag{36}$$

Hence, replacing θ_0 in (36) with any angle θ which belongs to the no-go zone, we have the boundary function of the reachable set $\mathbf{G}_\infty$:

$$v_u = \alpha(\theta) = \frac{dL(\theta_L - \theta)}{m \tan \delta_r}, \text{with } |\theta| \leq \theta_L. \tag{37}$$

A vessel with a velocity $v_u > \alpha(\theta)$ can always go across the no-go zone (see proof in [13]), otherwise it will be "in irons".

Accordingly, the entering velocity v_u must be larger than $v_{u\min}$, which is defined as the minimum velocity required to cross the no-go zone at $\theta = -\theta_L$, or the maximum longitudinal velocity in the reachable set:

$$v_{u\min} := \frac{2dL\theta_L}{m \tan \delta_r}. \tag{38}$$

2) Boundary Function $\beta(\theta)$: On the other hand, when the sailing vessel is outside the no-go zone, i.e. when $|\theta| > \theta_L$, (24) simplifies into

$$\dot{\theta}(t) = \frac{v_u(t)}{L}\tan\delta_r(t) \tag{39}$$

$$\dot{v}_u(t) = \frac{d}{m}(v_s(t) - v_u(t)). \tag{40}$$

Since $v_s(t) \geq v_u(t)$, equation (40) implies that $\dot{v}_u \geq 0$ at all time, i.e. the sailing vehicle is either in acceleration or constant velocity. When the vehicle is approaching the no-go zone but with $v_u(t) < v_{u\min}$, it must be accelerated in a short time to exceed $v_{u\min}$ before entering the no-go zone so that the vehicle will be guaranteed to cross it safely.

Then, assuming initial condition v_{u0}, the solution of (40) is

$$v_u(t) = v_{u0}e^{-\frac{d}{m}t} + v_s(1 - e^{-\frac{d}{m}t}), \tag{41}$$

which gives

$$\dot{\theta} = \frac{\tan\delta_r}{L}\big(v_{u0}e^{-\frac{d}{m}t} + v_s(1 - e^{-\frac{d}{m}t})\big). \tag{42}$$

Integrating both sides of (42), we have

$$\theta(t) = \frac{(v_{u0} - v_s)m\tan\delta_r}{dL}(1 - e^{-\frac{d}{m}t}) + \frac{v_s\tan\delta_r}{L}t + \theta_0. \tag{43}$$

In order to get the boundary function that guarantees the vehicle is driven from the initial state (θ_0, v_{u0}) to the final state $(-\theta_L, v_{u\min})$, let $v_u(t) = v_{u\min}$ in (41), and define t_L as the time it takes to reach $v_{u\min}$, starting from v_{u0}. Thus, we have

$$t_L(v_{u0}) = -\frac{m}{d}\ln\big(\frac{v_{u\min} - v_s}{v_{u0} - v_s}\big), \tag{44}$$

and substitute $\theta(t) = -\theta_L$ in (43), so that θ_0 can be isolated as

$$\begin{aligned}\theta_0 \;=\; & \frac{(v_{u0} - v_s)m\tan\delta_r}{dL}(e^{-\frac{d}{m}t_L(v_{u0})} - 1) \\ & - \frac{v_s\tan\delta_r}{L}t_L(v_{u0}) - \theta_L\end{aligned} \tag{45}$$

Hence, the boundary of the reachable set outside the no-go zone ($|\theta| > \theta_L$) can be represented by the function

$$\begin{aligned}\theta(v_u) \;=\; & \frac{(v_u - v_s)m\tan\delta_r}{dL}(e^{-\frac{d}{m}t_L(v_u)} - 1) \\ & - \frac{v_s\tan\delta_r}{L}t_L(v_u) - \theta_L,\end{aligned} \tag{46}$$

where

$$t_L(v_u) = -\frac{m}{d}\ln\big(\frac{v_{u\min} - v_s}{v_u - v_s}\big). \tag{47}$$

Thus, the boundary function can be described as a function $v_u = \beta(\theta)$ (with $|\theta| > \theta_L$), which is the inverse function of (46).

With the same parameters as those used in (24), the boundary of reachable set expressed by both functions $\alpha(\theta)$ and $\beta(\theta)$ are shown in Fig. 8 with reachable set $\mathbf{G}_\infty$. The comparison indicates that the reachable set by computing the subzero level set of the viscosity solution of HJ PDE (21) is quite accurate,

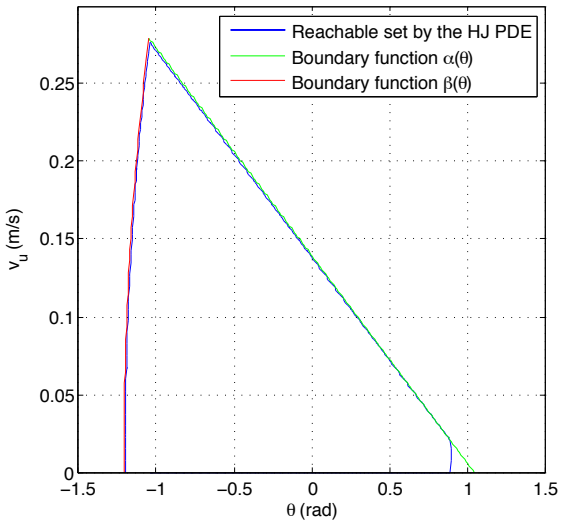

Fig. 8. Comparison of the reachable set from the calculation of the HJ PDE and its validations of the deadzone model

except for the absent space between θ'_L and θ_L, which is expected and is less important in the overall behavior of the system.

D. Lift/Drag model reachability analysis

We now compute numerically the reachable set for the lift/drag model, from which we extract the following dynamics

$$\begin{aligned}\dot{\mathbf{x}} &= \frac{d}{dt}\begin{bmatrix}\theta \\ v_u\end{bmatrix} = \begin{bmatrix}\frac{v_u}{L}\tan\delta_r \\ \frac{1}{m}\big(F_u(\theta(t), v_u(t), \bar{\delta}_s(t)) - dv_u(t)\big)\end{bmatrix} \\ &= f(\mathbf{x}, \delta_r, \bar{\delta}_s)\end{aligned} \tag{48}$$

which leads to the following Hamiltonian

$$\begin{aligned}H(\mathbf{x}, p) &= \max_{\delta_r}[p^T f(\mathbf{x}, \delta_r, \bar{\delta}_s)] = p^T f(\mathbf{x}, \bar{\delta}_r, \bar{\delta}_s) \\ &= p_1\frac{v_u}{L}\tan\bar{\delta}_r + \frac{p_2}{m}\big(F_u(\theta(t), v_u(t), \bar{\delta}_s(t)) - dv_u\big),\end{aligned} \tag{49}$$

where $\rho = 1.2\text{kg/m}^3$, $S = 3\text{m}^2$, and the maximum sail angle is fixed $\bar{\delta}_s = \pi/3\text{rad}$, the other parameters being the same as for the deadzone model.

Moreover, for the lift/drag model, the target set is the state with longitudinal velocity $v_u = 0$ and a heading angle in the interval $[-\bar{\delta}_s, \bar{\delta}_s]$. So the target set is the line segment between $(-\bar{\delta}_s, 0)$ and $(\bar{\delta}_s, 0)$, i.e. mathematically, we have

$$\begin{aligned}\mathbf{G}_0 &= \{\mathbf{x} \in (-\bar{\delta}_s \leq \theta \leq \bar{\delta}_s) \times (v_u = 0) \mid g(\mathbf{x}) \leq 0\}, \\ g(\mathbf{x}) &= \max(|v_u|, |\theta| - \bar{\delta}_s).\end{aligned} \tag{50}$$

Using a similar reasoning as in (27), $\mathbf{G}_0$ can be re-written as

$$\begin{aligned}&\mathbf{G}_0 = \{\mathbf{x} \in (-\bar{\delta}_s \leq \theta \leq \theta') \times (0 \leq v_u \leq v'_u) \mid g(\mathbf{x}) \leq 0\ \}\ , \\ &g(\mathbf{x}) = \max\left(\left|\theta - \frac{\theta' - \bar{\delta}_s}{2}\right| - \frac{\theta' + \bar{\delta}_s}{2}, \left|v_u - \frac{v'_u}{2}\right| - \frac{v'_u}{2}\right),\end{aligned} \tag{51}$$

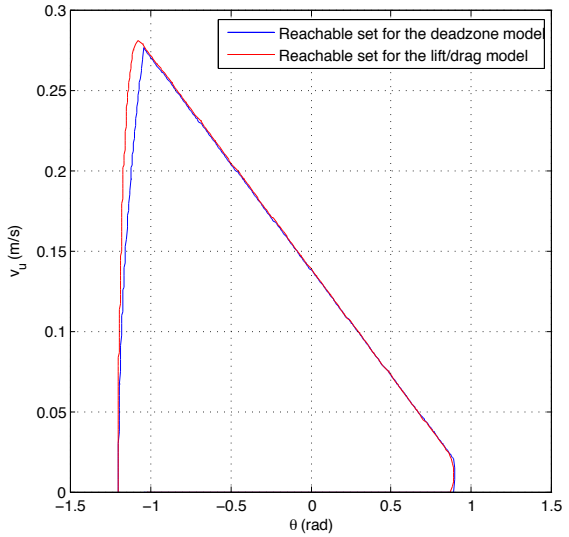

Fig. 9. Comparison of the reachable sets for the two models by the calculation of PDEs

where $v'_u = 0.02$ and $\theta' = 0.8972$.

During simulation, the stopping condition $H(\mathbf{x}, \frac{\partial \phi}{\partial \mathbf{x}}(\mathbf{x}, t)) \approx 0$ occurs around $\tau = 90s$. The backward reachable set $\mathbf{G}_\infty$ for the lift/drag model is shown in Fig. 9 against that of the deadzone model. The major difference in Fig. 9 is that the rising curve of the lift/drag model is a little higher than that of the deadzone model in the interval around $(0.13, 0.28)$ on the v-axis (when the vehicle is approaching the no-go zone), due to the more complex dynamics of v_u in the lift/drag model. Besides this, the reachable sets are quite similar, which, in a sense, confirms the validity of the deadzone model.

IV. Concluding remarks

This paper reported on a study of the validation of the simple deadzone model proposed by Jouffroy [1], by comparing its backward reachable set to that of a lift/drag model with respect to the no-go zone, which is a very important dynamic behavior during a tacking maneuver. A time dependent Hamilton-Jacobi PDE was used to compute the reachable sets for these two models. The almost identical backward reachable sets in Fig. 9 illustrate that, even though the dynamics of v_u in the lift/drag model is more advanced, the simpler deadzone model has very similar characteristics during a tack. However, because of its relative simplicity, using the deadzone model could be an advantage and more convenient to handle for automatic control purposes or path planning for sailing vehicles.

References

[1] J. Jouffroy, "A control strategy for steering an autonomous surface sailing vehicle in a tacking maneuver," in *Conf. on Systems, Man, and Cybernetics*, San Antonio, Texas, 2009.

[2] ——, "On steering a sailing ship in a wearing maneuver," in *IFAC International Conference on Maneuvering and Control of Marine Craft*, Guaruja, Brazil, 2009, pp. 26–31.

[3] I. M. Mitchell, A. M. Bayen, and C. J. Tomlin, "A time-dependent hamiltoncjacobi formulation of reachable sets for continuous dynamic games," *Transactions on Automatic Control*, vol. 50, no. 7, pp. 947–957, Jul 2005.

[4] T. I. Fossen, *Marine control systems: guidance, navigation and control of ships, rigs and underwater vehicles*. Marine Cybernetics, 2002.

[5] C. A. Marchaj, *Aero-hydrodynamics of sailing*. Adlard Coles Nautical, 1979.

[6] P. J. Richard, A. Jonson, and A. Stanton, "America's cup downwind sail-vertical wings or horizontal parachutes?" *Journal of Wind Engineering and Industrial Aerodynamics*, vol. 89, pp. 1565–1577, 2001.

[7] I. Mitchell and C. J. Tomlin, "Overapproximating reachable sets by hamiltoncjacobi projections," *J. Scientific Comput.*, vol. 19, no. 1-3, pp. 323–346, 2003.

[8] L. C. Evans and P. E. Souganidis, "Differential games and representation formulas for solutions of hamiltoncjacobicisaacs equations," *Indiana Univ. Math. J.*, vol. 33, no. 5, p. 773C797, 1984.

[9] M. G. Crandall, L. C. Evans, and P.-L. Lions, "Some properties of viscosity solutions of hamiltoncjacobi equations," *Trans. Amer. Math. Soc.*, vol. 282, no. 2, pp. 487–502, 1984.

[10] S. Osher and R. Fedkiw, *Level Set Methods and Dynamic Implicit Surfaces*. New York: Springer-Verlag, 2002.

[11] S. Osher and J. A. Sethian, "Fronts propagating with curvature-dependent speed: Algorithms based on hamilton-jacobi formulations," *J. Comput. Phys.*, vol. 79, pp. 12–14, 1988.

[12] I. Mitchell. (2007, Jun.) A toolbox of level set methods (version 1.1). [Online]. Available: http://www.cs.ubc.ca/ mitchell/ToolboxLS/

[13] L. Xiao and J. Jouffroy, "Reflexions on feedforward control strategies for a class of sailing vehicles," in *8th IFAC Conference on Control Applications in Marine Systems (CAMS)*, Rostock-Warnemnde, Germany, Sep 2010.